energies

Article

Energy Intake Models for Intermittent Operation of Dead-End Microfiltration Filling Line †

Jure Ravnik [1,‡], Gorazd Bombek [1,‡], Aleš Hribernik [1,‡], Timi Gomboc [1,‡], Matej Zadravec [1,‡], Aleks Kapun [2,‡], Grega Hrovat [2,‡], Jure Gradišek [2,‡] and Matjaž Hriberšek [1,*,‡]

[1] Faculty of Mechanical Engineering, University of Maribor, Smetanova 17, SI-2000 Maribor, Slovenia
[2] Technical Research and Development, Global Drug Development, Novartis, Lek d.d., SI-1234 Mengeš, Slovenia
* Correspondence: matjaz.hribersek@um.si
† This article is dedicated to Professor Paul Steinmann on the occasion of his 60th birthday.
‡ These authors contributed equally to this work.

Abstract: In filling lines equipped with membrane separation devices in the form of filters energy, consumption is only one of the important working parameters, the other being sustainable filter performance in terms of separation efficiency. As the filling line is typically equipped with a valve, intermittent operation of the filter is an important form of its use. Whereas the overall energy consumption of the filtration process is governed by the continuous operation mode, the intermittent mode, characterised by opening/closing of the valve, contributes most to problems of filter failure, i.e., the breakthrough of filtered particles through the membrane. A model for determination of the energy intake of a microfiltration membrane during the opening and closing of a valve is presented in this work. The model is based on computational analysis of the pressure wave signals recorded during the opening/closing of the valve using Fourier transform, and expressed in a nondimensional filter area specific energy intake form. The model is applied to a case of constant pressure dead-end microfiltration with three filter types: a single membrane filter, a stacked filter and a pleated filter with filtration surface areas ranging from 17.7 cm^2 to 2000 cm^2. Both clean filters, as well as partially clogged filter cases are taken into account. Second order polynomial models of the energy intake are developed and evaluated based on extensive analysis of the experimental data. The analysis of energy intake results show that the largest energy intake was observed for the clean filter case. When membrane fouling occurs at the constant flow rate values it leads to larger energy intake, however, due to a decreasing specific flow rate during fouling these values do not exceed the clean filter case.

Keywords: membrane filtration; water hammer effect; membrane energy intake; filter clogging

check for updates

Citation: Ravnik, J.; Bombek, G.; Hribernik, A.; Gomboc, T.; Zadravec, M.; Kapun, A.; Hrovat, G.; Gradišek, J.; Hriberšek, M. Energy intake models for intermittent operation of dead-end microfiltration filling line. *Energies* **2022**, *15*, 8854. https://doi.org/10.3390/en15238854

Academic Editor: Mahmoud Bourouis

Received: 21 October 2022
Accepted: 21 November 2022
Published: 23 November 2022

Publisher's Note: MDPI stays neutral with regard to jurisdictional claims in published maps and institutional affiliations.

1. Introduction

Filtration is one of the most important separation processes in process engineering. It is used in many industries [1] using filter membranes of different designs and properties. In this paper, we focus on the problem of filter membrane load due to water hammer [2] pressure surges caused by the opening or closing of the valve in the filtration pipeline. The cause of the pressure surge is a sudden change in the momentum of the fluid. This phenomenon occurs when a valve suddenly closes or opens, slowing down or accelerating the liquid and creating a pressure wave that spreads through the pipe and hits the filter membrane. It is well known that filter membranes clog during operation due to one of the fouling mechanisms. When a pressure surge reaches a partially fouled membrane, it is possible for the membrane to fail and allow some of the filtered material to break through the membrane, hence contaminating the product. This type of event is more likely if the water hammer pressure surge hits the membrane not once, but several tens or hundred times. This is especially important in the case of dead-end filtration, where the whole kinetic

energy of the flow is transformed into pressure energy. In the industrial environment this is often the case when the surge tank that collects the filtrate is small, and therefore needs to be emptied regularly. Each time the surge tank is emptied, a valve, positioned behind the filter, must be opened, and later closed again, causing water hammer pressure surges on the filter membrane. In a filtration process, the blocking of membrane pores, i.e. filter fouling, leads to an increase of membrane hydraulic permeability, and, hence, during operation at constant pressure, to a decrease of filtrate flow rate. The problem of filter fouling has been researched extensively in recent years. For example, Laska et al. [3] argued that tests with laboratory scale filters are very important for a correct design of production scale devices. Iritani and Katagiri [4,5] gave an excellent review of different blocking fouling laws proposed by researchers, describing complete blocking law, standard blocking law, intermediate blocking law, and cake filtration law. Bolton et al. [6,7], on the other hand, argued that a combination of fouling models best describes the physical processes occurring in the membrane. Bowen et al. [8] studied the flow decline due to membrane blocking during protein microfiltration. Fallahianbijan et al. [9] exposed the importance of pore interconnectivity for virus filtration. Peles et al. [10] examined the effect of operating pressure on fouling during constant pressure filtration. Water hammer effects [11] have also been studied extensively in a wide variety of systems. Li et al. [12] considered the water hammer effect during hydraulic fracturing. Xi et al. [13] considered the water hammer in an annular channel, and found that the water hammer pressure forms a double imbalance in the internal and external walls of eccentric annulus tubing. Water hammer in a viscoelastic pipe was studied by Zhang et al. [14]. Their experimental results showed that the maximum water hammer pressure generated in the viscoelastic pipe at all flow velocities was (20% at most) greater than the traditional value of Joukowsky's formula. Water supply systems were considered by Lyu et al. [15], who showed that an appropriate water hammer protective scheme is very important in water supply systems. Water hammers can cause cavitation, as shown by Jansson et al. [16] by means of a high speed camera. Aslam et al. [17] have shown that the water hammer effect can be used to prevent membrane fouling. Considering whey protein ultrafiltration they achieved up to 84% flux enhancement. Similarly, Broens et al. [18] also proposed to use the water hammer effect to mitigate membrane fouling during ultrafiltration of natural water. When the pressure waves hit the filtration membrane, the incoming waves are partially reflected, partially transmitted through the membrane and partially absorbed by the membrane itself. This leads to the effect that there is a part of the incoming pressure energy that hits the interior of the membrane, where it can give rise to additional pressure related forces, acting on filtrated particles. These forces can act as a trigger for the particles to reorient and/or partially deform, and in this way penetrate deeper into the membrane. Finally, when the number of pressure hammer occurrences exceeds a critical level a breakthrough phenomenon occurs, leading to contamination of the product, which is especially critical in the case of pharmaceutical applications. Since an in-depth experimental or computational analysis of particle–membrane-structure interaction is extremely difficult to perform, tracking integral parameters, i.e., pressures at the membrane inlet and membrane outlet, can be used, in order to develop some integral criteria that could help in the analysis of contamination problems of membrane filtration across different scales, from a laboratory to the production scale. In the present work, the filtration process is studied by means of energy consumption. In [19] energy consumption for the case of dead-end ultrafiltration was studied, with the goal of developing a minimised energy consumption control strategy. As in the case of microfiltration, almost all of the pressure drop occurs across the membrane, and the energy consumption can also be regarded as an energy intake into the membrane. In view of this, in this work the energy intake criterion for a microfiltration case is developed and evaluated experimentally for different types of filters, including laboratory and production type filters.

2. Materials and Methods

2.1. Fluid Flow through a Micromembrane Filter

Flow through a filtration membrane can be modelled as a flow through the saturated porous media (i.e. a porous open solid structure, fully filled with the single phase fluid). When the local fluid velocities are low, a linear drag model for the drag force, excerted by the fluid on the porous structure, is valid. The linear drag model is the core of the Darcy flow model, i.e.,

$$\vec{v}_f = -\frac{\mathbf{K}}{\eta}\vec{\nabla}p \tag{1}$$

with $\vec{v}_f = (v_{fx}, v_{fy}, v_{fz})$ the fluid (filtrate) velocity, Δp the pressure drop, η the filtrate dynamic viscosity and $\mathbf{K}$ the hydraulic permeability tensor of the porous medium. If we assume the flow direction is aligned with the conduit direction (i.e. the channel, in which the filter is inserted), isotropic filter properties and flow velocities low enough for the Darcy model (Equation (1)) to be valid, the average flow velocity through the filter is defined as

$$v_F = \frac{\dot{V}}{A} \tag{2}$$

The v_F is commonly referred to also as the filtration rate J defined as the filtrate flow rate per unit area of the filter, i.e.,

$$J = \frac{\dot{V}}{A} \tag{3}$$

The filtration rate can also be expressed in terms of pressure drop Δp and filter resistance R as

$$J = \frac{\Delta p}{\eta R} \tag{4}$$

with R

$$R = \frac{\Delta L}{K} \tag{5}$$

The role of the micromembrane is to block the passing of the particulate phase while allowing the fluid phase to flow through. As the particulate phase is being held by the membrane, this, in turn, starts to limit the flow performance of the filter, as the accumulation of the particulate phase gives rise to several phenomena with a common effect—the increase of the filter resistance to filtrate flow, also known as filter clogging or membrane fouling. As the filtration rate J at the constant pressure operating conditions decreases during the filtration process, so also does the hydraulic permeability K, or, in the case of constant filtration rate conditions the pressure drop increases, leading again to a decrease in K. In either case, the K is a function of either the pressure or the filtration rate, which both depend on the filtration time or volume of filtrate:

$$K = f_1(\Delta p, J) = f_2(t) = f_3(V) \tag{6}$$

The same holds also for the filtration rate and the filtrated volume V , i.e.,

$$\dot{V}(t) = f_1(\Delta p, K) = f_2(t) = f_3(V) \tag{7}$$

with V calculated as a sum over the entire duration of the filtration process, i.e.,

$$V = \int_0^t \dot{V} dt = \sum_i \dot{V}_i \Delta t_i \tag{8}$$

During constant pressure operation of the filter one can model the flow rate variation with time $\dot{V}(t)$ using two parameters and one of the four fouling models. We introduce the

initial flow rate $\dot{V}_0$ and the maximal filtrate volume V_{max} as model constants, to express the flow rate for the four fouling modes [5] with

$$\dot{V}(t) = \dot{V}_0 \exp\left(-\frac{\dot{V}_0 t}{V_{max}}\right), \quad \text{complete blocking,} \tag{9}$$

$$\dot{V}(t) = \dot{V}_0 \frac{1}{\left(1+\frac{\dot{V}_0 t}{V_{max}}\right)^2}, \quad \text{standard blocking,} \tag{10}$$

$$\dot{V}(t) = \dot{V}_0 \frac{1}{1+\frac{\dot{V}_0 t}{V_{max}}}, \quad \text{intermediate blocking,} \tag{11}$$

$$\dot{V}(t) = \dot{V}_0 \frac{1}{\sqrt{1+2\frac{\dot{V}_0 t}{V_{max}}}}, \quad \text{cake filtration.} \tag{12}$$

The model constants are typically determined by analysing a dataset of a sample of laboratory scale filtration of the targeted suspension.

2.2. Energy Intake in Membrane Filtration

The pressure drop across the membrane gives rise to normal pressure force acting on the membrane. As the membrane material is typically some type of organic polymer, material stretching can occur, leading to a change in the pore sizes, as well as pore size aspect ratios' distributions [20]. Typically, an increase in pore sizes can be observed. The constitutive behaviour of such membrane materials could be defined as viscoelastic-rate-independent plastic, which means that plastic deformations can arise during membrane filtration operation, altering the membrane permeability, but also, and most importantly, altering membrane selectivity. A general trend in view of permeability is that the membrane stretching increases pore sizes, and this leads to an increase in membrane permeability. On the other hand, the effect of the increased pore sizes results in a degradation of membrane performance, i.e., its selectivity. The extent of plastic deformations that can arise during membrane filtration operation can be linked to the energy intake on the membrane, which takes place under continuous flow conditions and intermittent flow conditions.

2.2.1. Continuous Flow Operation of the Filter

The energy consumed by the process of filtration is a consequence of the overcoming of the resistance of the filtration media under a specific volumetric flow rate, marking the continuous flow operation of the filter. Examining the power consumption , describing energy intake per unit time, it is obvious that, indeed, the power intake depends on the transmembrane pressure difference Δp and the $\dot{V}$ the flow (filtration) rate,

$$P_f = \Delta p \; \dot{V} = P_f(t) \tag{13}$$

In both filtration operating conditions, constant pressure as well as constant flow rate, one of the two parameters is constant and the other one is time dependent. In the case of constant pressure conditions the Δp is a constant value, while the filtration rate is decreasing with time; in the case of constant filtration rate, i.e., constant flow conditions, the pressure drop increases due to increasing of the filter resistance with time. If specific values are to be considered, then the filtration (membrane) area specific power consumption is defined as

$$P_{f,s} = \Delta p \; \frac{\dot{V}}{A} \tag{14}$$

Rearranging gives

$$P_{f,s} = J \; \Delta p = P_{f,s}(t) \tag{15}$$

If the overall energy intake per membrane filtration area is sought, the time integration is needed to yield the result:

$$E_{f,s} = \int_0^T J\ \Delta p\ dt \tag{16}$$

with T the filtration time.

2.2.2. Intermittent Flow Operation of the Filter

When it comes to intermittent flow conditions at the start of the full valve closure the pressure hammer effect leads to a sudden increase of the pressure in the outlet pipe, and, consequently, also at the membrane outlet surface and across the membrane depth. The pressure wave that arrives at the membrane is partially reflected, partially absorbed and partially transmitted through the membrane. The reflective wave gives rise to additional pressure waves in the outlet pipe, and, hence, an additional transmembrane pressure difference Δp, which, typically, decreases to zero during the transition period. On the other hand, when the filtration is resumed, instead of the closing of the valve the opening of the valve creates a similar effect. To resume, both valve operations create fluctuations of pressure on both sides of the membrane, that lead to additional forces on the fluid as well as on the filtered material in/on the membrane, that can create a creeping flow of the filtered particles towards the downstream side of the membrane, and, consequently, lead to contamination of the filtrate. As the energy intake due to continuous operation can be calculated accurately by evaluating the Equation (16), under intermittent flow conditions with no flow through the membrane, another approach must be derived.

2.2.3. Water Hammer Effect in Membrane Filtration

When, during the filtering operation in a pipeline system a valve is suddenly closed, a resultant pressure wave propagates through the pipe. The peaks in pressure are a result of the fluid's inertia, with conversion of the kinetic energy of the fluid into a pressure energy when the valve is closed. According to the formula of Joukowsky the pressure surge is calculated as:

$$\Delta p_{wh} = \rho_f c_w \Delta v \tag{17}$$

with c_w speed of sound in the medium and Δv the change in average velocity. The maximum expected pressure surge is achieved when the change in velocity is equal to the average velocity of the flow, i.e., $\Delta v = \dot{V}(t)/A$, with A being the pipe cross-section.

$$\Delta p_{wh} = \rho_f c_w \frac{\dot{V}(t)}{A}, \tag{18}$$

where time t is measured from the start of the filtering operation. When it comes to intermittent flow conditions, the filtrate flow rate at the start of the full valve closure is essentially equal to zero; however, the pressure hammer effect leads to a sudden increase of the pressure in the outlet pipe, and, consequently, also at the membrane outlet surface and across the membrane depth. The pressure wave that arrives at the membrane is partially reflected, partially absorbed and partially transmitted through the membrane. The reflective wave gives rise to additional pressure waves in the outlet pipe, and, hence, additional transmembrane pressure difference Δp, which, typically, decreases to zero during the transition period. On the other hand, when the filtration is resumed, instead of the closing of the valve the opening of the valve creates a similar effect, with resulting pressures reaching much lower levels at the outflow side of the membrane than in the closing case. To resume, both valve operations create fluctuations of pressure on both sides of the membrane, that lead to additional forces on the fluid, as well as on the filtered material in/on the membrane, that can create a creeping flow of the filtered particles towards the downstream side of the membrane, and, consequently, lead to contamination of the filtrate. The energy intake of the membrane can be associated with the resulting membrane deformation, the workload on the filtered particles, which are not rigid, and

can be deformed due to the action of the oscillating pressure field, as well as with viscous dissipation, transforming the energy of the fluid into heat. An exact computation of the absorbed energy by the membrane, as well as pressure forces and deformations on the filtered particles, would be connected with in-depth mechanical modelling of the inner viscoplastic porous structure of the filtration membrane and 3D elastoplastic response of the filtered particles, which is currently out of the scope of this work. However, under the assumption of a constant absorption rate and constant rate of absorbed pressure-related workload on the particles, the evaluation of the overall intake of the pressure wave energy can serve as a good reference value for the derivation of a filter failure criterion. In this paper, we focus on experimental measurements of pressure oscillations occurring after valve manipulations, and propose a method of determining the filter membrane energy intake due to these events.

2.3. Experimental Setup

The experimental system is presented schematically and in photographs in Figures 1 and 2. Compressed gas (nitrogen) is connected to the top of the pressure vessel partly filled with the selected testing fluid, in order to obtain the pressure head necessary to transport the fluid through the filter. A fine adjustable reduction valve is applied at the gas tank, in order to select and maintain a constant feed pressure. A flexible pipe is used to connect the pressure vessel to the testing section. Tri-clamp connectors are used for a quick filter exchange. A temperature sensor (Pt100, Hart Scientific 1504) and two piezoelectric pressure sensors Type 601 CAA with Charge Amplifiers 5015A from Kistler are applied, in order to measure the fluid temperature and pressure ahead of (p1) and behind (p2) the filter. A narrow pipe (l = 200 mm, D = 10 mm) with a quick closing solenoid valve (2/2 way angle-seat valve Type 2000 from Buerkert fluid control systems) at the end of it, is connected to the testing section to generate a fluid hammer effect and study any influence it may have on the filtration process. An LVDT type position sensor from the RDP Group was applied to measure the valve's position. It was connected directly to the valve stem through the upper housing opening. A weighting scale (Kern KB 650 2N) and a three-way solenoid valve for precise selection of measuring time period, when necessary, are applied at the system outflow for the steady-state flow rate measurements.

A computer-aided measurement system (National Instruments Compact RIO System) was applied for temperature, pressure and valve lift measurements, as well as for the solenoid valve control and the scale reading, while the feed pressure setting was performed manually. The measuring and control algorithm were programmed in LabVIEW (National Instruments). There were two setups. The slow one was running on an RT (Real Time) processor. This setup is used for quasi steady state measurements such as mass flow rate or filter clogging measurements. The scale is connected via RS-232 communication. The pressure signal can be current or voltage. The valve (digital signal) can be controlled via a mouse click or programmatically (N cycles at a desired time interval). The sampling frequency was set to 10 Hz and floating average filtering was applied for temperature, pressure and filtered volume measurement under steady-state testing conditions. Time critical measurements such as pressure oscillations were performed on an FPGA with a 50 kHz sampling frequency. In this case, simultaneous acquisition of current and voltage signals was performed in conjunction with valve control (digital output). Scale reading and/or temperature can be recorded only once per measuring procedure. Several openings and closing of the valve can be acquired during one measuring procedure, but they were limited mostly to 1 or 2 cycles to avoid memory issues. The NIcRIO 9014/9104 controller/chassis and NI 9215, NI 9203 and NI 9282 modules were used). Any signal post-processing, such as filtering, FFT and similar was performed by standard LabVIEW routines. The testing procedure started with filling the pressure vessel with the selected testing fluid through the pressurising gas pipe, since no extra filling aperture was foreseen in order to keep the system compact. At the same time, the venting valve at the top of the vessel was opened. Once full, the vessel was closed and connected to the pressurised gas and the

testing section was filled with the fluid. Any trapped air was removed through the venting holes in the filter casing, and then the feed pressure was set to the selected level. Once the feed pressure and fluid temperature stabilised and the steady state conditions were reached, the measurement was carried out. An example of the measured data acquired during a dynamic single membrane laboratory filter test is given in Figure 3. The testing procedure was fully automated. After the selected time interval, the solenoid valve opened, filtration started, and the measuring system acquired signals from the applied sensors. The acquisition time was limited to the first 1 to 2 s, while the valve remained opened until the pressure fluctuations calmed down when the solenoid valve was closed and the signals acquisition of the valve closing process took place.

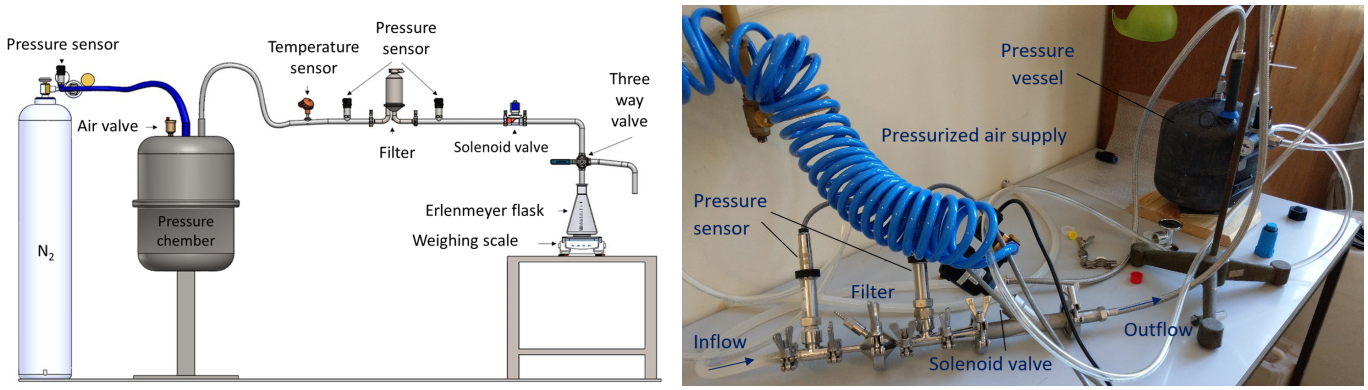

Figure 1. Experimental setup.

Figure 2. Filter casing (**left**) and support plate (**right**).

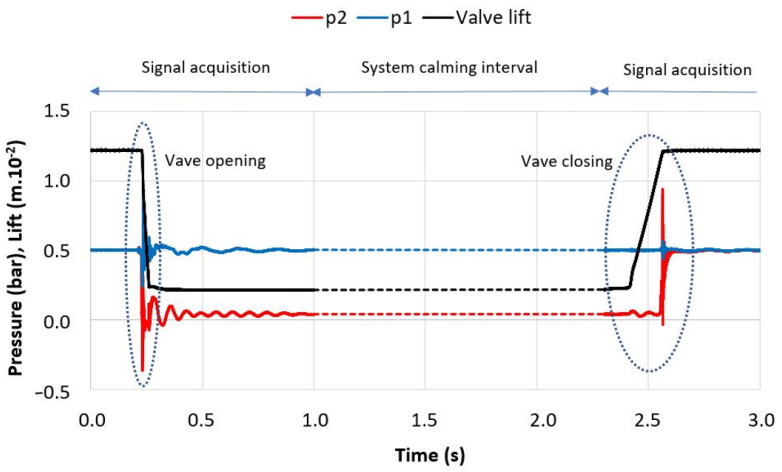

Figure 3. Pressure ahead and behind the filter (p_1 and p_2, respectively) and solenoid valve lift variation versus time acquired during single membrane laboratory filter dynamic test.

2.4. Energy Intake Calculation

2.4.1. A Single Steady State Wave

One possibility of calculating the energy intake in intermittent conditions is to calculate the power transmitted by the pressure wave to the porous material. Let us consider a pressure wave in a fluid travelling in the x direction. As the first step, let the wave be steady, i.e., its amplitude and frequency do not change with time. The displacement of fluid particles when the wave travels through them is

$$s(x,t) = s_{max}\cos(kx - \omega t + \phi), \tag{19}$$

where $k = 2\pi/\lambda$ is the wave number, $\omega = 2\pi\nu$ is the frequency, and ϕ is the phase. The change in pressure is related to displacement via the compressiblity of the fluid χ and relative change in volume:

$$\Delta p(x,y) = -\chi^{-1}\frac{dV}{V} = -\chi^{-1}\frac{\partial s(x,t)}{\partial x} = \underbrace{\chi^{-1}ks_{max}}_{\Delta p_{max}}\sin(kx - \omega t + \phi) = \Delta p_{max}\sin(kx - \omega t + \phi) \tag{20}$$

The pressure oscillates with amplitude p_{max}, which depends on the wavelength, compressibility and displacement. The velocity at which the fluid elements (not the wave) are moving is derived from the displacement as

$$v(x,t) = \frac{\partial s(x,y)}{\partial t} = s_{max}\omega\sin(kx - \omega t + \phi) \tag{21}$$

Let P denote the power, i.e., the rate at which energy is transferred by the wave. Intensity I is the power through an area A. Since power is force times the velocity, we may write

$$I(x,t) = \frac{P}{A} = \frac{Fv}{A} = \Delta p(x,y)v(x,y) = \chi^{-1}k\omega s_{max}^2\sin^2(kx - \omega t + \phi) \tag{22}$$

Since intensity is time dependent, we calculate the time averaged intensity of a wave in a period $2\pi/\omega$:

$$I(x) = \frac{\omega}{2\pi}\int_0^{2\pi/\omega} I(x,t)dt = \frac{k\omega s_{max}^2}{2\chi} = \frac{\omega^2 s_{max}^2}{2\chi c_w} = \frac{(\Delta p_{max})^2}{2\rho_f c_w}, \tag{23}$$

where we used the density of the fluid ρ_f, the travelling speed of the waves $c_w = \sqrt{1/\chi\rho_f}$, the pressure amplitude $\Delta p_{max} = \chi^{-1}ks_{max}$ and $\omega = kc_w$ to find that the intensity of a pressure wave is proportional to the change in the pressure squared and inversely proportional to the density and the speed. Considering the difference in intensity before the filter I_b and after I_a, we can calculate the energy transferred to the filter in time period T as

$$\frac{E}{A} = E_s = \frac{1}{2\rho_f c_w}\int_{t=0}^{T}\left|(\Delta p_{a,max})^2 - (\Delta p_{b,max})^2\right|dt \tag{24}$$

Here E_s is the filter area specific energy intake measured in J/m^2. Equation (24) is valid for a single pressure wave that behaves like (20).

2.4.2. Several Steady State Waves

Closing or opening of the valve results in a myriad of waves all moving together in the direction of the filter. To decompose the pressure time trace into individual waves we used the Fourier transform. The Fourier transform yields the amplitude Δp_{max} for each wave

contained in the detected signal, allowing the Equation (20) to be used for each frequency, and finally summing the result to obtain the total energy intake from all waves as:

$$I_b = \frac{1}{2\rho_f c_w}\sum_i (\Delta p_{b,max,i})^2, \qquad I_a = \frac{1}{2\rho_f c_w}\sum_i (\Delta p_{a,max,i})^2 \tag{25}$$

$$\frac{E}{A} = E_s = \int_{t=0}^{T} |I_b - I_a| dt = \frac{1}{2\rho_f c_w}\int_{t=0}^{T} \sum_i \left| (\Delta p_{a,max,i})^2 - (\Delta p_{b,max,i})^2 \right| dt \tag{26}$$

where $\Delta p_{a,max,i}$ is the amplitude of the wave with i-th frequency.

2.4.3. Unsteady Pressure Waves

The measured and simulated pressure-time traces before and after the filter reveal that the waves propagating in the fluid change with time. The reasons for this are the reflection of the waves and non-instantaneous generation of the waves. This means that we should reveal how the intensity difference changes with time. To take this into account we used the moving window approach, to capture the time variation in the composition of the pressure waves. Thus, the energy intensity at time t before the membrane $I_b(t)$ and after the membrane $I_a(t)$ were calculated by taking a short data sample centred at t, and using FFT to decompose the signal into individual waves. Considering the frequency composition of the pressure time traces we should choose an FFT sample length long enough to capture all relevant frequencies, and, at the same time, the sampling rate should be high enough to ensure that all energy has been accounted for. We found during testing that the ratio of intensities I_b/I_a was revealed correctly, even if the sampling rate was not high enough to capture all frequencies. To test this procedure, we considered an analytic expression for the pressure signal before and after the filter defined as a composition of three waves with frequencies 1.0 Hz, 99.9 Hz, 222.2 Hz and amplitudes 4 Pa, 2 Pa and 3 Pa, respectively. We assumed that, after the filter, the signal amplitude was diminished by a factor of 2. For such a setting, the difference in intensity before and after the filter was

$$2\rho_f c_w (I_b - I_a) = \left(\sum_{i=1}^{3} (\Delta p_{b,max,i})^2 - \sum_{i=1}^{3} (\Delta p_{b,max,i})^2 \right) = 21.75\ Pa^2 \tag{27}$$

To calculate the intensity difference, it is essential that we identify individual waves and their amplitudes correctly. The Fourier transform, which was used for this task, can do this only when the signal is of sufficient length compared to the wavelength of the pressure waves. To verify this, we prepared data files by sampling the test signals with a time step of 10^{-3} s for several periods of different lengths. Using these data files, we calculated the spectra using FFT, and recovered the intensity results presented in Table 1. We observed that when the sample length was longer than 1 s we obtained the correct values for the intensity. This limit corresponded to the lowest frequency in the signal, which was 1 Hz. We can conclude that the intensity is recovered correctly only if the length of the signal which is used to perform the spectral analysis is longer than one wavelength of the shortest wave.

Since, to capture the time variation of our signal, we would like to keep the size of the moving window as short as possible, we concluded that it is not possible to use the intensity difference to measure energy intake accurately. However, the results in Table 1 also revealed that the ratio of intensities I_b/I_a was captured accurately regardless of the moving window size. Thus, we decided to introduce a nondimensional measure for energy intake based on the ratio of intensities. It is described in the next sub-section. Nevertheless, the calculation of dimensional filter area-specific energy intake E_s using Equation (26) is useful for comparing designs when recorded and evaluated consistently. The specific energy intake obtained, for example, using experiments conducted at a consistent and fixed sampling rate combined with FFT analyses with a consistent and fixed moving window size, were comparable to each other, and can provide a measure for total energy intake. The

values were under-predicted, as explained above, but were under-predicted in a consistent manner, and, thus, can be used for comparison purposes.

Table 1. Dependance of calculated intensity on sample length.

Sample Length $[ms]$	$I_b \cdot 2\rho_f c_w$ $[Pa^2]$	$I_a \cdot 2\rho_f c_w$ $[Pa^2]$	$(I_b - I_a) \cdot 2\rho_f c_w$ $[Pa^2]$	I_b/I_a $[-]$
analytical	29	7.25	21.75	4
16384	29.07	7.26	21.81	4.004
4096	28.71	7.18	21.53	3.999
2048	28.65	7.16	21.49	4.001
1024	28.66	7.16	21.50	4.003
512	22.43	5.61	16.82	3.998
256	22.67	5.68	16.99	3.991
128	16.53	4.13	12.40	4.002

2.4.4. Nondimensional Measure for Energy Intake

Instead of using eq. (26) we proposed a nondimensional filter area specific energy intake E_s' as

$$E_s' = \int_0^T \Delta I_s'(t)dt, \qquad \Delta I_s'(t) = \frac{|I_b - I_a|}{\max(I_a, I_b)} w(t), \qquad w(t) = \frac{|I_b - I_a|}{\int_0^T |I_b - I_a| d\tau} \tag{28}$$

where the E_s' non-dimensional filter area specific energy intake, $\Delta I_s'(t)$ $[s^{-1}]$ is the specific intake intensity and w_i is the weight. The weight was added to the definition, so E_s' is susceptible to the magnitude of the energy intake. Without it, the energy intake of a low energy wave would count the same as the energy intake of a high energy wave. To understand the physical meaning of the non-dimensional filter area specific energy intake E_s' let us consider a simple relationship that the filter attenuates the signal intensity for a constant factor of α, $0 < \alpha < 1$, i.e. $I_a = \alpha I_b$. When we evaluate (28) we obtain:

$$E_s' = \frac{1}{\int_0^T (I_b - I_a) d\tau} \int_0^T \frac{(I_b - I_a)^2}{I_b} dt = \frac{(1-\alpha)^2}{(1-\alpha)} = 1 - \alpha \tag{29}$$

Thus, when the filter diminishes the signal intensity by a factor of α, the resulting non-dimensional energy intake is $E_s' = 1 - \alpha$. This means that the filter area specific energy intake is limited between 0 and 1, at $0 \leq E_s' \leq 1$. At $E_s' = 0$ the filter does not take any energy from the pressure waves, at $E_s' = 1$, the filter absorbs all the energy of the pressure wave and no wave is transmitted through the filter.

2.4.5. Algorithm

We propose the following algorithm to calculate the energy intake:

- use a moving window approach to analyse the complete pressure time series before and after the filter. The length of the moving window does not influence the results, so we choose so that it is long enough to capture most of the frequencies in the signals and at the same time short enough to still resolve time variation of the signal.
- Loop over the whole signal using the moving window
  - use the Fourier transform to decompose the pressure signal before and after the filter membrane into individual waves and calculate the amplitude of each wave $\Delta p_{max,i}$
  - calculate the intensity for each wave in the spectrum using Equation (23)
  - get the total intensity before and after the filter by summing contributions of individual wave Equation (25)
  - calculate the specific intake intensity $\Delta I_s'(t)$ for each time step using Equation (28)

- perform the integral (26) using numerical quadrature to obtain the dimensional filter area specific energy intake E_s.
- perform the integral (28) using numerical quadrature to obtain the nondimensional filter area specific energy intake E'_s.

3. Results

Both laboratory and industrial scale filters were analysed, and tests were performed with clean, semi-clogged and clogged filters, respectively. Distilled water was used for the tests, while tap water, stored in an uncleaned vessel, was applied to clog the selected filter prior to the clogged filter testing. Two single-membrane laboratory scale filters from Pall Corporation were tested: Fluorodyne II DFL (FTKDFL) and Fluorodyne EX EDF (FTKEDF), both having 0.2 μm removal rating and an 14 cm^2 nominal effective filter area. The Fluorodyne EX grade EDF filters are 0.2 micron rated high capacity, low protein binding sterilizing grade filters. They contain a built-in pre-filtration layer (a high-capacity asymmetric polyether sulfone (PES)) over a polyvinylidene fluoride (PVDF) membrane layer. They are validated to retain Brevundimonas diminuta bacilli at a rate of ten million colony forming units per square centimetre of filter. The Fluorodyne EX grade EDF filters are ideal for sterile filtration of cell harvest material and biological process fluids. They are used in the pharmaceutical industry, since the asymmetic PES membrane before the PVDF membrane improves the filter capacity and delays clogging. As such, they are the focus of our research. The Fluorodyne II DFL features a polyvinylidene fluoride (PVDF) dual layer membrane. Furthermore, two industrial filter units were used, i.e., an in-line stainless steel filter housing with filter cartridge. The first was a Junior Filter Cartridge—MCY Style from Pall Corporation (MCY4440DFLPH4), which features a pleated Fluorodyne II 0.2 μm filter (PL) with a PVDF dual layer membrane, 0.2 μm removal rating and 1500 cm^2 nominal effective filter area. The second was a Stacked - Millidisk 40 Cartridge 0.22 μm filter (ST) from Millipore Corporation (MCGL40S03). This filter contains hydrophilic, Durapore® polyvinylidene fluoride (PVDF) membranes with an 0.22 μm removal rating and 2000 cm^2 total nominal effective filter area. We considered the following filters and scenarios: an EFL single membrane laboratory filter: clean (EDF), semi-clogged (EFL-CLG-20) and clogged (EFL-CLG), a DFL single membrane laboratory filter: clean (EDF) and clogged (EFL-CLG), a pleated filter (PL) and a stacked filter (ST) and a clogged stacked filter (ST-CLG).

3.1. Dimensional and Non-Dimensional Energy Intake

In this section, we present the results of the energy intake calculation for the chosen filters, performed using the presented algorithm. The energy intake was calculated by integrating the specific intake intensity over time. We observed similar behaviour in all cases: A large spike in the specific intake intensity at the time of valve opening or closing, when the first pressure waves travelled through the filter. The energy intake subsided afterwards as the rebounding waves were attenuated by the filter. To understand the results, we present the results in the form of the following plots: the pressure signal captured before and after the filter, the specific intake intensity as a function of time, and wave intensity and wave amplitude spectra. As an example, these plots are presented in Figure 4 for a horizontal filter set-up. We can confirm clearly that substantial energy intake takes place only immediately after the valve manipulation. The Table 2 compares dimensional and non-dimensional energy intakes for laboratory scale filters for different cases. Similarly, the Table 3 present the results of energy intake analysis for stacked and pleated filters at a pressure difference of 0.5 bar. We observed low non-dimensional energy intake for cases without flow. In such cases, a pressure surge caused by valve manipulation was absorbed poorly by the filter membrane. When flow was present, the energy intake was significantly larger. This was especially noticeable with valve closing, where, in all cases, the non-dimensional energy intake was larger than 90%. This means that most of the energy carried by the pressure waves gets absorbed by the filter membrane. Looking at the dimensional energy intake it was observed that it depends strongly on the valve

orientation. Furthermore, when a 10% sucrose solution was filtered instead of water, a significant increase was observed in the energy intake.

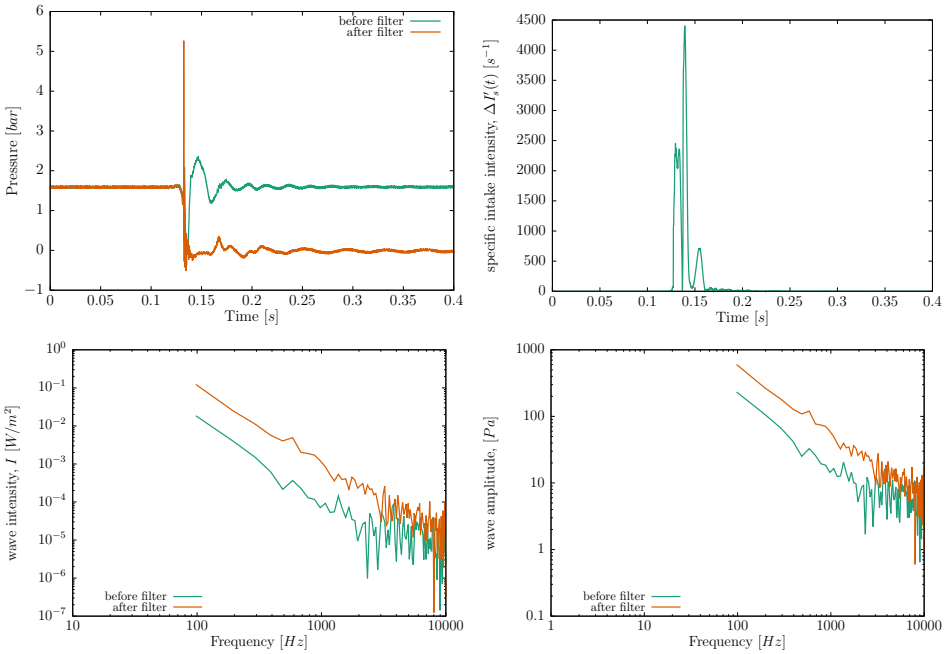

Figure 4. Case: valve opening, experimental results for horizontal set-up. In the (**top left**) panel pressure signal captured before and after the filter is shown. Specific intake intensity versus time is shown in (**top right**). (**Bottom row**): wave intensity and wave amplitude spectra.

Table 2. Dimensional (E_s) and non-dimensional (E'_s) specific energy intake for all experimental cases with laboratory scale filters. The dimensional specific energy intake was calculated using time resolution of 20 μs and 100 μs and moving window size 512 for experimental measurements.

Valve	Comment	E'_s [−]	E_s [J/m^2]
opening	horizontal, no flow	0.516	23.3
opening	vertical, no flow	0.570	31.7
opening	horizontal	0.774	41.8
opening	vertical	0.630	37.2
opening	horizontal, flipped	0.753	11.3
opening	sucrose 15%	0.932	59.3
closing	horizontal, no flow	0.582	1.4
closing	vertical, no flow	0.228	0.4
closing	horizontal	0.929	5.1
closing	vertical	0.958	3.4
closing	horizontal, flipped	0.929	3.7
closing	sucrose 15%	0.983	10.9

Table 3. Dimensional (E_s) and non-dimensional (E_s') specific energy intake for all experimental cases. The dimensional specific energy intake was calculated using time resolution of 20 μs and moving window size of measurements. $\Delta p = 0.5$ *bar* in all cases.

Valve	Comment	E_s' $[-]$	E_s $[J/m^2]$
opening	pleated	0.857	1.99
opening	stacked	0.884	2.47
opening	stacked, clogged	0.936	1.66
closing	pleated	0.783	1.1
closing	stacked	0.739	3.0
closing	stacked, clogged	0.932	1.69

3.2. Specific Flow Rate versus System Pressure

Although the producers of micromembrane filters provide basic data on specific flow rate vs. applied pressure, it is, nevertheless, necessary to conduct experimental tests to determine this relationship for the tested filtration system, including the micromembrane filter, in order to have as accurate as possible information for the tested system. Therefore, determination of the specific flow rate $J = \dot{V}/A$ was conducted for all the applied filters with a pressure range between 0.1*bar* and 1*bar*. A linear relationship was, as expected, confirmed in all cases, with two examples shown in Figure 5, with linear fits for all cases given in Table 4.

Table 4. Models for specific flow rate valid for system pressure in the rage of $0.1 < \Delta p < 1$. Experiments based on which the models were developed were performed with distilled water.

Case Name	Eq. for J $[mL/(dm^2 s)]$, p $[bar]$
lab. filter, DFL	$11.15457719 \cdot p - 0.10493360$
clogged lag. filter, DFL-CLG	$6.72255315 \cdot p - 0.10423828$
lab. filter, EDF	$14.71983783 \cdot p - 0.13740174$
semi-clogged lab. filter, EDF-CLG-20	$10.75590313 \cdot p + 0.13670827$
clogged lab. filter, EDF-CLG	$9.17365272 \cdot p - 0.01143736$
pleated filter, PL	$12.82900476 \cdot p + 0.00955190$
stacked filter, ST	$13.73365810 \cdot p + 0.26570152$
clogged stacked filter, ST-CLG	$5.98012740 \cdot p - 0.30930602$

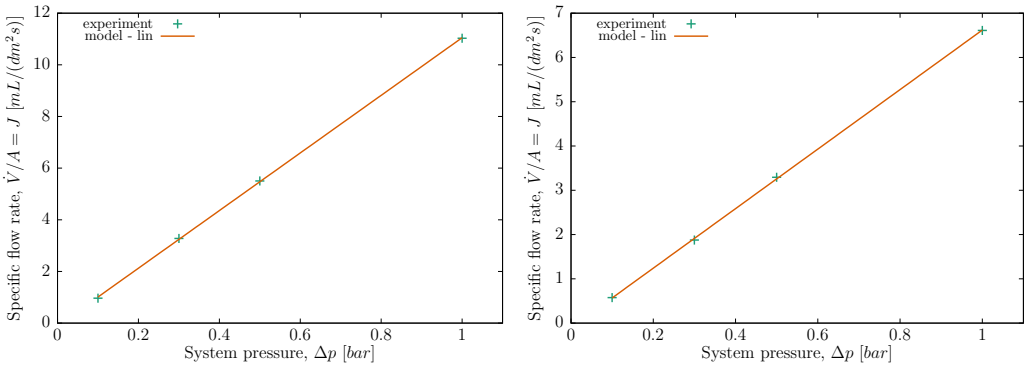

Figure 5. Experimental and modelled system pressure versus specific flow rate curves; (**left**) DFL, (**right**) DFL-CLG.

3.3. A Model for Energy Intake due to Valve Closing and Opening

To develop energy intake models, a series of experiments was performed for a DFL filter (clean and clogged), an EDF filter (clean, semi-clogged and clogged), a pleated filter (PL) and a stacked filter (ST, clean and clogged). Four system pressures were considered: 0.1 *bar*, 0.3 *bar*, 0.5 *bar* and 1.0 *bar*. Each of the experiments was repeated three times, and the energy intake was calculated for all cases. Figure 6 presents the average energy

intakes and standard deviations for all cases. We observed that energy intake increased with system pressure for both valve opening and valve closing cases. For each case we developed a fit of the energy intake data versus the system pressure, and versus the specific flow rate. Linear, parabolic, power low, exponential and logarithmic fits were considered. The one with the lowest difference between the fit and the data was considered as the energy intake model. Table 5 and the associated Figures display all the developed model equations and present the models graphically.

Table 5. Models for specific energy intake during valve opening and closing. Experiments based on which the models were developed were performed with distilled water and 2-1 valve configuration.

Case Name	opn/cls	Eq. for E/A $[J/m^2]$, p $[bar]$, J $[mL/(dm^2 s)]$	Validity
lab. filter DFL	opn	$14.46340664 \cdot p^2 - 4.17941366 \cdot p + 2.75539303$	$0.1 < p < 1$
	opn	$0.11832034 \cdot J^2 - 0.37073540 \cdot J + 2.73845151$	$1 < J < 11$
	cls	$1.38943965 \cdot p^2 + 0.19291081 \cdot p + 0.61767057$	$0.1 < p < 1$
	cls	$0.01152869 \cdot J^2 + 0.01564509 \cdot J + 0.62556357$	$1 < J < 11$
clogged lab. filter DFL	opn	$7.26535392 \cdot p^2 + 3.23692415 \cdot p + 1.35367715$	$0.1 < p < 1$
	opn	$0.16322356 \cdot J^2 + 0.50008037 \cdot J + 1.41572060$	$1 < J < 7$
	cls	$0.64009916 + 0.08056488 \cdot \exp(2.52528529 \cdot p)$	$0.1 < p < 1$
	cls	$0.02420608 \cdot J^2 + -0.02576759 \cdot J + 0.75805301$	$1 < J < 7$
lab. filter EDF	opn	$14.18963433 \cdot p^2 - 7.96757375 \cdot p + 3.26147328$	$0.1 < p < 1$
	opn	$0.06579624 \cdot J^2 - 0.52573868 \cdot J + 3.18314941$	$1 < J < 15$
	cls	$-1.39313133 \cdot p^2 + 4.82595490 \cdot p + 0.14713774$	$0.1 < p < 1$
	cls	$-0.00600348 \cdot J^2 + 0.31873297 \cdot J + 0.21211857$	$1 < J < 15$
semi clogged lab. filter EDF-CLG-20	opn	$12.66335105 \cdot p^2 - 4.05132936 \cdot p + 1.69409557$	$0.1 < p < 1$
	opn	$0.12221813 \cdot J^2 - 0.53173285 \cdot J + 1.88331213$	$1 < J < 11$
	cls	$-1.45022341 \cdot p^2 + 5.49542759 \cdot p + 0.03727903$	$0.1 < p < 1$
	cls	$-0.00536575 \cdot J^2 + 0.42300443 \cdot J + 0.15648571$	$1 < J < 11$
clogged lab. filter EDF-CLG	opn	$23.81311264 \cdot p^2 - 20.14513114 \cdot p + 7.66142189$	$0.1 < p < 1$
	opn	$0.28630691 \cdot J^2 - 2.17704352 \cdot J + 7.48379093$	$1 < J < 9$
	cls	$-12.90644442 \cdot p^2 + 18.68459258 \cdot p - 0.44731903$	$0.1 < p < 1$
	cls	$-0.14238979 \cdot J^2 + 1.89592982 \cdot J - 0.13589408$	$1 < J < 9$
pleated filter PL	opn	$7.24736718 \cdot p^2 - 2.12629159 \cdot p + 1.20618395$	$0.1 < p < 1$
	opn	$0.04281711 \cdot J^2 - 0.14964926 \cdot J + 1.16941196$	$1 < J < 13$
	cls	$4.99257169 \cdot p^2 - 2.71316633 \cdot p + 1.20083424$	$0.1 < p < 1$
	cls	$0.02914738 \cdot J^2 - 0.19468491 \cdot J + 1.16097125$	$1 < J < 13$
stacked filter ST	opn	$0.63707195 + 0.13845305 \cdot \exp(5.27453812 \cdot p)$	$0.1 < p < 1$
	opn	$0.05523568 + 0.40591994 \cdot \exp(0.27744038 \cdot J)$	$1 < J < 12$
	cls	$-0.69998754 + 0.76909910 \cdot \exp(3.18656760 \cdot p)$	$0.1 < p < 1$
	cls	$0.06702557 \cdot J^2 + 0.01665472 \cdot J + 0.01972929$	$1 < J < 12$
clogged stacked filter ST-CLG	opn	$0.15099263 + 0.37255856 \cdot \exp(2.66825096 \cdot p)$	$0.1 < p < 1$
	opn	$0.25327646 + 0.35786070 \cdot \exp(0.47425980 \cdot J)$	$1 < J < 6$
	cls	$2.98450498 \cdot p^{1.13513598}$	$0.1 < p < 1$
	cls	$-0.00460393 \cdot J^2 + 0.55238816 \cdot J + -0.02146555$	$1 < J < 6$

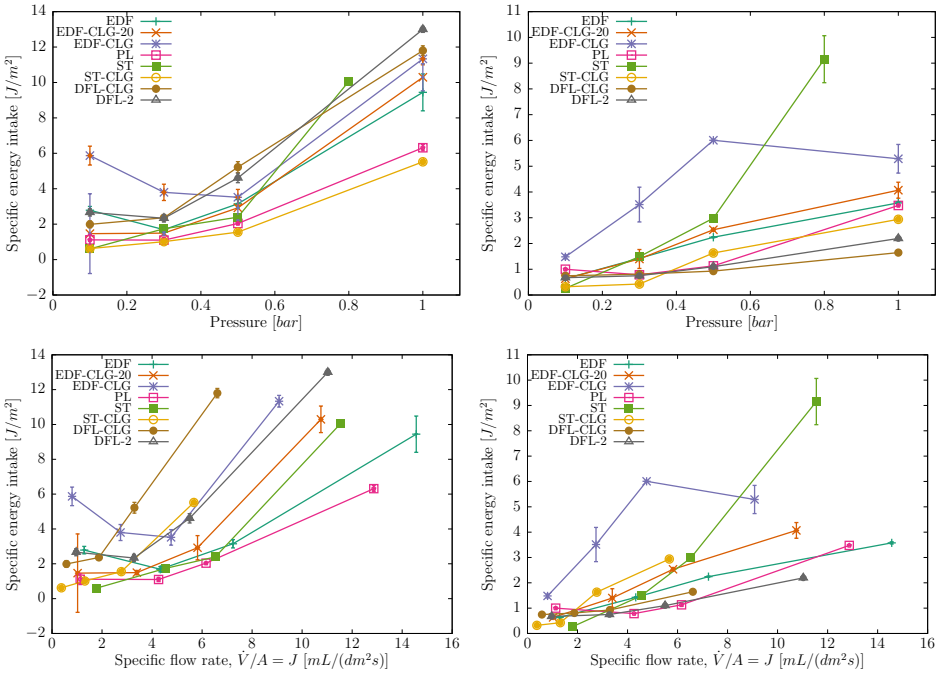

Figure 6. Specific energy intake versus applied pressure difference (**top row**) and versus specific flow rate (**bottom row**) for all cases, (**left**)—valve opening, (**right**)—valve closing.

As the main energy intake should arise from the change in kinetic energy of the decelerating or accelerating flow, it is to be expected that the specific energy intake should increase with the increasing specific flow rate values. Indeed, almost all of the data show this trend, with a few exceptions:

- At the lowest system pressures (0.1 *bar*) the trends are not completely clear or even a decrease in energy intake with flow rate can be observed. It has to be emphasized that the implemented pressure sensors had the working range of 0*bar* and 2*bar*, with 0.1*bar* at the very lowest part of the useful range. This can lead to inaccuracies in recording the pressure oscillations and hence in calculating the energy intake values.
- The EDF-CLG 40% clogged case shows an uncharacteristic peak of the energy intake at 0.5*bar*, followed by a decrease at higher flow rates, which should be attributed to some undetermined system disturbance rather than physically relevant cause.
- The derived model functions are of various types, including polynomial and exponential functions. These functions do approximate the covered pressure and specific flow rate range very accurately. However, due to their numerical nature they should be used with care when applied outside the tested range.
- When the derived downscale models would intended to be used above the tested range, i.e., for extrapolation purposes, a conservative approach would be to replace the functions with linear model approximations.

The results also reveal the impact of filter fouling/clogging. When one compares the trends the following observations can be made:

- When the energy intake is compared at the same system pressure conditions a general trend in all clogged cases is a significant decrease of the energy intake, valid for the opening as well as the closing of the valve. This is attributed to a decrease in the flow rate, a direct effect of filter clogging.
- When the energy intake is compared at the same system specific flow rate (J) conditions a general trend in all clogged cases is an increase of energy intake, valid for the opening as well as the closing of the valve. This is attributed to an increase in filter hydraulic resistance, a result of filter clogging, which additionally lowers the filter hydraulic permeability.

- With a known filter fouling model, i.e., one of the models in Equation (9), one can now calculate an overall energy intake for a case of intermittent operation with filter fouling.

The energy intake is a consequence of pressure drop oscillations across the membrane These oscillations result from two sources:

- from kinetic energy of the flow, that comes to rest or is accelerated due to the action of the valve,
- from the action of the valve itself, as its movement displaces the fluid and produces pressure forces even in the case of no flow.

In the case of laboratory scale filters the action of the valve itself can play a significant role, with its specific closing/opening mechanism, where repeatability of its actions cannot be controlled. This effect diminishes in the case of industrial filters, where a much larger fluid volume is present between the membranes and the valve, with much more complex downstream internal channels, contributing to a lower impact of the valve action on the energy intake.

3.4. On the Use of Developed Energy Intake Models for Downscale Data Transfer

The question now arises of how to use the developed models—should we consider the full fouling behaviour of the filter when working with product formulation, or could the data obtained from the distilled water case at clean filter conditions, be an adequate substitute, or even a worst case scenario? For the first test case we considered the energy intake of the DFL filter by implementing the developed models. The system pressure was set at $\Delta p = 0.4\ bar$. We assumed 10 valve manipulations, during which the flow rate diminished to that which corresponds to the system pressure of $\Delta p = 0.1\ bar$, emulating filter clogging from an initial clean state. The system pressure versus flow rate relationship was used to calculate the flow rates. For the DFL filter we obtained (see Table 4):

- $4.35\ mL/(dm^2 s)$ at $\Delta p = 0.4\ bar$ for the initial (clean) state of the filter,
- $0.56\ mL/(dm^2 s)$ at $\Delta p = 0.1\ bar$ for the clogged state after 10 manipulations,
- let us assume that valve manipulations occur at regular intervals, so that the flow rate decreases from $4.35\ mL/(dm^2 s)$ to $0.56 mL/(dm^2 s)$ linearly.

We now calculated the energy intake for two cases:

- Clean filter case: consider the same flow rate of $4.35\ mL/(dm^2 s)$ for all valve manipulation events and use the developed model for the clean filter to estimate the energy intake.
- Clogged filter case: consider a linearly decreasing flow rate from $4.35\ mL/(dm^2 s)$ to $0.56\ mL/(dm^2 s)$ and evaluate the energy intake at different flow rate using the model developed for the clogged filter.

The results show that the resulting energy intake for both cases was of the same order of magnitude ($42.8\ J/m^2$ for the clean DFL case and $47.5\ J/m^2$ for the clogged DFL case). We repeated this analysis for the stacked filter as well. A similar conclusion was discovered; the energy intake for both cases was of the same order of magnitude ($44.0\ J/m^2$ for the clean stacked filter and $39.2\ J/m^2$ for the clogged stacked filter).

We can conclude that using the clean filter flow rate and E_s model to estimate energy intake for all valve manipulations gives a result which is comparable to the real case of filter clogging and decreasing flow rate, hence, that using the energy intake characteristics of the clean filters at the specific flow rates, which were decreasing in the clogged case, led to roughly the same specific energy intake. Based on this conclusion, we developed the downscale models using clean filter models only. It must be emphasised that the use of clean filter characteristics is possible only for the case of constant pressure operation, and not for the case of constant volume flow rate operation. For the latter case the fouling has to be considered, as filter clogging and the corresponding decrease of membrane permeability lead to higher energy intake values

4. Conclusions

The energy intake models based on the extensive experimental testing of various filter types were designed, developed and validated in this paper. Several aspects of the study are worth summarising. In the experiments we encountered issues with system venting. The entrapment of air in the system influenced the dynamics of the pressure field in the case of closing the valve significantly, as the presence of air increased the value of compressibility of the liquid in the system. The valve closing effects in this case extended in time compared with the clear water case. The difference in the specific energy intake was also analysed in the case of distilled water vs. higher density product formulations. Two test cases were considered at the laboratory scale, with the use of a 15% water sucrose solution with 6% higher density than water. The DFL filter case showed higher energy intake values than the distilled water case, whereas the EDF filter showed the opposite trend, with differences in the range of approx. $\pm$20%. The findings on specific energy intake on production filters vs. laboratory filter were as follow. The stacked, as well as pleated filters, in general exhibited a lower specific energy intake in closing/opening than filters at the laboratory scale at the same levels of specific flow rates. When studying specific energy intake in the case of partially clogged membranes we found that, in all the tested clogged cases, where fouling of membranes was achieved experimentally, the energy intake in the clogged state at a constant pressure conditions was significantly lower than in the case of a clean filter, for both opening, as well as closing of the valve. When the energy intake was compared at the same system specific flow rate (J) conditions, a general trend in all clogged cases was an increase of the specific energy intake, valid for the opening, as well as the closing of the valve. Finally, the energy intake model functions for clean filters, developed based on extensive experimental data, may, therefore, serve as an aid in the modelling of filter breakthrough phenomena, if combined with empirical data on registered breakthrough events in targeted filtration systems.

Author Contributions: Conceptualization, J.R. and M.H.; methodology, J.R., M.H., G.B., A.H., T.G. and M.Z.; software, J.R. and G.B.; validation, G.B., T.G. and M.Z.; formal analysis, M.H.; investigation, T.G., A.K., G.H. and J.G.; writing—original draft preparation, J.R. and M.H.; writing—review and editing, J.R., A.H. and M.H.; visualization, G.B. and J.R.; supervision, A.K., G.H. and J.G.; project administration, M.H.; funding acquisition, M.H. All authors have read and agreed to the published version of the manuscript.

Funding: This research was funded by the Slovenian Research Agency (Research core funding No. P2-0196), and Lek d.d under the Contract No. BIO11-2019.

Data Availability Statement: Not applicable.

Conflicts of Interest: The funders had no role in the design of the study; in the collection, analyses, or interpretation of data; in the writing of the manuscript; or in the decision to publish the results.

Abbreviations

The following abbreviations are used in this manuscript:

DFL	Pall corporation laboratory scale filter Fluorodyne II DFL
EDF	Pall corporation laboratory scale filter Fluorodyne EX EDF
FFT	fast Fourier transform
FPGA	field programmable gate array
LVDT	linear variable differential transformer
PES	symmetric polyether sulfone
PVDF	polyvinylidene fluoride
CLG	clogged
PL	pleated filter
ST	stacked filter

References

1. Nigam, M.O.; Bansal, B.; Chen, X.D. Fouling and cleaning of whey protein concentrate fouled ultrafiltration membranes. *Desalination* **2008**, *218*, 313–322. https://doi.org/10.1016/j.desal.2007.02.027.
2. Sarker, S.; Sarker, T. Spectral Properties of Water Hammer Wave. *Appl. Mech.* **2022**, *3*, 799–814. https://doi.org/10.3390/applmech3030047.
3. Laska, M.E.; Brooks, R.P.; Gayton, M.; Pujar, N.S. Robust scale-up of dead end filtration: Impact of filter fouling mechanisms and flow distribution. *Biotechnol. Bioeng.* **2005**, *92*, 308–320. https://doi.org/10.1002/bit.20587.
4. Iritani, E. A Review on Modeling of Pore-Blocking Behaviors of Membranes During Pressurized Membrane Filtration. *Dry. Technol.* **2013**, *31*, 146–162. https://doi.org/10.1080/07373937.2012.683123.
5. Iritani, E.; Katagiri, N. Developments of blocking filtration model in membrane filtration. *KONA Powder Part. J.* **2016**, *2016*, 179–202. https://doi.org/10.14356/kona.2016024.
6. Bolton, G.; LaCasse, D.; Kuriyel, R. Combined models of membrane fouling: Development and application to microfiltration and ultrafiltration of biological fluids. *J. Membr. Sci.* **2006**, *277*, 75–84. https://doi.org/10.1016/j.memsci.2004.12.053.
7. Bolton, G.R.; Boesch, A.W.; Lazzara, M.J. The effects of flow rate on membrane capacity: Development and application of adsorptive membrane fouling models. *J. Membr. Sci.* **2006**, *279*, 625–634. https://doi.org/10.1016/j.memsci.2005.12.057.
8. Bowen, W.; Calvo, J.; Hernandez, A. Steps of membrane blocking in flux decline during protein microfiltration. *J. Membr. Sci.* **1995**, *101*, 153–165.
9. Fallahianbijan, F.; Giglia, S.; Carbrello, C.; Zydney, A.L. Quantitative analysis of internal flow distribution and pore interconnectivity within asymmetric virus filtration membranes. *J. Membr. Sci.* **2020**, *595*, 117578. https://doi.org/10.1016/j.memsci.2019.117578.
10. Peles, J.; Fallahianbijan, F.; Cacace, B.; Carbrello, C.; Giglia, S.; Zydney, A.L. Effect of operating pressure on protein fouling during constant-pressure virus removal filtration. *J. Membr. Sci.* **2022**, *648*, 120351. https://doi.org/10.1016/j.memsci.2022.120351.
11. Choon, T.W.; Aik, L.K.; Aik, L.E.; Hin, T.T. Investigation of Water Hammer Effect Through Pipeline System. *Int. J. Adv. Sci. Eng. Inf. Technol.* **2012**, *2*, 246. https://doi.org/10.18517/ijaseit.2.3.196.
12. Li, Y.; Hu, X.; Zhou, F.; Qiu, Y.; Li, Z.; Luo, Y. A new comprehensive filtering model for pump shut-in water hammer pressure wave signals during hydraulic fracturing. *J. Pet. Sci. Eng.* **2022**, *208*, 109796. https://doi.org/10.1016/j.petrol.2021.109796.
13. Xi, B.; Wang, C.; Xi, W.; Liu, Y.; Wang, H.; Yang, Y. Experimental investigation on the water hammer characteristic of stalling fluid in eccentric casing-tubing annulus. *Energy* **2022**, *253*, 124113. https://doi.org/10.1016/j.energy.2022.124113.
14. Zhang, X.; Chen, S.; Xu, T.; Zhang, J. Experimental study on pressure characteristics of direct water hammer in the viscoelastic pipeline. *J. Water Supply Res. Technol.-Aqua* **2022**, *71*, 563–576. https://doi.org/10.2166/aqua.2022.005.
15. Lyu, J.; Zhang, J.; Wang, T. Study on water hammer protection of the siphon breaking structure in the water supply system. *J. Water Supply Res. Technol.-Aqua* **2022**, *71*, 478–489. https://doi.org/10.2166/aqua.2022.162.
16. Jansson, M.; Andersson, M.; Karlsson, M. High-Speed Imaging of Water Hammer Cavitation in Oil–Hydraulic Pipe Flow. *Fluids* **2022**, *7*, 102. https://doi.org/10.3390/fluids7030102.
17. Aslam, M.; Wicaksana, F.; Farid, M.; Wong, A.; Krantz, W.B. Mitigation of membrane fouling by whey protein via water hammer. *J. Membr. Sci.* **2022**, *642*, 119967. https://doi.org/10.1016/j.memsci.2021.119967.
18. Broens, F.; Menne, D.; Pothof, I.; Blankert, B.; Roesink, H.D.; Futselaar, H.; Lammertink, R.G.; Wessling, M. Water hammer reduces fouling during natural water ultrafiltration. *Water Res.* **2012**, *46*, 1113–1120. https://doi.org/10.1016/j.watres.2011.12.011.
19. Blankert, B.; Kattenbelt, C.; Betlem, B.H.; Roffel, B. Dynamic optimization of a dead-end filtration trajectory: Non-ideal cake filtration. *J. Membr. Sci.* **2007**, *290*, 114–124. https://doi.org/10.1016/j.memsci.2006.12.024.
20. Siddiqui, M.U.; Arif, A.F.M.; Bashmal, S. Permeability-selectivity analysis of microfiltration and ultrafiltration membranes: Effect of pore size and shape distribution and membrane stretching. *Membranes* **2016**, *6*, 40. https://doi.org/10.3390/membranes6030040.